ARTICLE

School of Material and Energy, Guangdong University of Technology, Guangzhou 510006, P. R. China. Email: hxzhx@sina.com (X. Feng.)
NSFC Center for Luminescence from Molecular Aggregates, SCUT-HKUST Joint Research Laboratory, State Key Laboratory of Luminescent Materials and Devices, South China University of Technology, Guangzhou 510640, P. R. China. Email: msqinaj@scut.edu.cn (A. J. Qin)
Beijing Institute of Graphic Communication, Beijing 102600, P.R. China.
Department of Chemistry, University of Hull, Cottingham Road, Hull, Yorkshire HU6
Laboratory for Soft Machines & Electronics, Michigan State University, East Lansing 48824, MI
Department of Chemistry and Hong Kong Branch of Chinese National Engineering Research Center for Tissue Restoration and Reconstruction, The Hong Kong University of Science & Technology, Kowloon, Hong Kong 999077, P. R. China; Shenzhen Institute of Molecular Aggregate Science and Engineering, School of Science and Engineering, The Chinese University of Hong Kong, Shenzhen 518172, China. Email: tangbenz@ust.hk (B. Z. Tang)
† Footnotes relating to the title and/or authors should appear here.
Electronic Supplementary Information (ESI) available: [details of any supplementary information available should be included here]. See DOI: 10.1039/x0xx00000x
Received 00th January 20xx,
Accepted 00th January 20xx

DOI: 10.1039/x0xx00000x

Pyrene-based Aggregation-induced Emission Luminogens (AIEgens) with less colour migration for Anti-counterfeiting Applications

Xiaohui Wang,[a] Lirong Wang,[b], Xiaoyu Mao,[a] Qingsong Wang,[a] Zhongfei Mu,[a] Li An,[c] Wan Zhang,[c] Xing Feng,[a*] Carl Redshaw,[d] Changyong Cao,[e] Anjun Qin,[*b] Ben Zhong Tang[*b,f]

Traditional luminescent materials are subject to aggregation-caused quenching, which limits their use for high-technological applications in the solid state. In an attempt to address such issues when using luminescent materials in fluorescence inks, by taking advantage of the aggregation-induced emission (AIE) behavior, this article presents a set of pyrene-based AIEgens which possess high thermal stability, excellent fluorescence properties, and good biocompatibility. These AIEgens can be utilized as fluorescence ink for anti-counterfeiting applications at ultralow/low concentration (0.004~0.5 wt%) (WeightAIEgens:Weightbinder = 5:125000~5:1000) with slight color migration (<27 nm) for different printing substrates. The use of such a fluorescence ink containing pyrene-based AIEgens has extended the scope of application over the range from ultralow to high concentration thereby avoiding the aggregation-caused quenching (ACQ) effect. Additionally, this system would lower the product cost, and be benefical for the environment. The high-quality fluorescence pattern was found to exhibit good printability on different types of paper by screen printing technology. This work highlights that pyrene-based AIEgens are excellent candidates for use in anti-counterfeiting, and these results have the potential to enrich the practical applications of AIEgens in both academic and industrial fields.

Introduction

Counterfeiting is a challenging global problem that causes huge economic losses and potential risk to individuals and social security.[1,2] Various advanced anti-counterfeiting technologies have been developed for fighting the fast-growing counterfeit markets.[3,4] Among them, the use of fluorescence labels/tags as a preferred anti-counterfeiting technology, has attracted great attention for practical application in banknotes, brands, and documents, because of their extraordinary superiority with regard to a fast response, visualization, and extra security features etc.[4-7] Thus, a large quantity of high fluorescence intensity/efficiency luminescent materials, including rare-earth-doped nanostructures,[8-10] carbon dots,[11-13] organic-inorganic complexes,[14-16] upconversion nanoparticles[17-18] and perovskite, [19-20] as well as organic dyes,[21-23] have been widely utilized as fluorescence labels/tags for printing technology.

Generally, the luminescent materials are used in the solid state for anti-counterfeiting applications, but the emission of traditional luminescent materials is subject to fluorescence quenching at high concentration or in the solid state, resulting in aggregation-caused quenching (ACQ).[24] The nature of conventional fluorescence dyes and their ACQ effect limits their practical application for anti-counterfeiting. For example, a low concentration of luminescent materials could achieve a weak anti-counterfeiting pattern, whilst a higher concentration not only lowers the emission intensity, but also adds to the production costs, as well as probably adding risks to the ecosystem. A significant milestone occurred in 2001 when Tang and coworkers found that a propeller-shaped molecule (such as tetraphenylethene, and siloles etc.) exhibited aggregation-induced emission (AIE) characteristics. [25] AIE is an impressive photophysical phenomenon, given that luminescent materials exhibit non or weak emission in solution but enhanced fluorescence intensity in the aggregation (solid) state, due to the restricted intramolecular motion (RIM) mechanism. More importantly, the development of AIE luminogens (AIEgens) led to significant advantages in emission efficiencies, biocompatibility, and light stability. [24-28]

As an excellent fluorophore, pyrene exhibits high fluorescence intensity and quantum yield, a long fluorescent lifetime and is extremely responsive to its micro-environment. These attributes mean that it is widely used to construct various organic luminescent materials for potential application in organic electronic, [29] chemsensors,[30] cell imaging,[31] etc. On the other hand, pyrene derivatives can also be used to prepare fluorescent inks for the preparation of fluorescence labels by writing and printing.[32-35] Much effort has been devoted to the functionalization of pyrene in order to improve the fluorescence properties.[36] Most of the efficient strategies involve transforming pyrene-based ACQ

conformation of the substituents.[37-40] For example, the integration of pyrene and tetraphenylethene results in high-performance pyrene-based AIE luminogens with blue emission and high quantum yield suitable for organic light emitting diode (OLED) fabrication.[41,42] Also, the cyanostyrene-type molecules are a well-known class of AIE/AIEE fluorophore, which have been widely applied in diverse areas, such as mitochondrial imaging, [43] mechanochromism, [44-46] and OLEDs. [47]

Generally, commercial inorganic fluorescence materials (inks) are composed of one or more metal elements, such as rare-earths,[48,49] or heavy metals,[50,51] which increases the cost of the products, as well as increasing the risk of environmental pollution. On the other hand, to realize the anti-counterfeiting application, the content of inorganic luminescent materials in fluorescence inks needs to be in range 0.1 wt% to 25 wt% according to previous reports, [52,53] whilst a higher content fraction of the fluorescence material would cause the fluorescence intensity to decrease due to the ACQ effect.[54] More importantly, the micro-environment of the content of the fluorescence ink plays a significant role to affect the chemical/physical properties of fluorescent pigments (such as chemical stability, color migration, etc.), resulting in low quality printing products/patterns. Thus, in this article, a set of new pyrene-based cyanostyrenes have been synthesized by introducing twisted bulky units, which exhibited clear AIE characteristic sky-blue or cyan emission. Subsequently, we attempted to use the pyrene-based AIEgens as functional fluorescent pigments to prepare fluorescence inks for anti-counterfeiting by screen-printing technology, which resulted in high-quality anti-counterfeiting at ultralow/low concentrations (0.004 ~ 0.5 wt%, $Weight_{AIEgens}$:$Weight_{binder}$ = 5:125000~5:5:1000) with relative small color migration (<27 nm) in butter paper and tissue paper substrate. Thus, this example opens up new avenues for the industrial application of pyrene-based AIEgens as anti-counterfeiting inks.

Results and discussion

Synthesis and characterization

The four pyrene-based cyanostyrene derivatives are presented in Figure 1, and all target compounds were obtained via two reaction steps (a Suzuki–Miyaura coupling reaction and a Knoevenagel reaction) in good yield. The detailed synthetic routes are illustrated in Scheme S1. The molecular structures of the compounds were fully characterized by $^{1}H/^{13}C$ NMR spectroscopy, high resolution mass spectrometry (HRMS) and single crystal X-ray diffraction. The relationship between the length of the π-conjugation (**Py-2Ph-Cz** and **Py-Ph-Cz**), the different substituents (**Py-Ph-Cz** and **Py-1-TPE**) or the substituent position (**Py-1-TPE** and **Py-2-TPE**) to the thermal properties, and the electronic spectra were systematically investigated by thermogravimetric analysis (TGA), UV-vis and fluorescence spectra, as well as by DFT calculations.

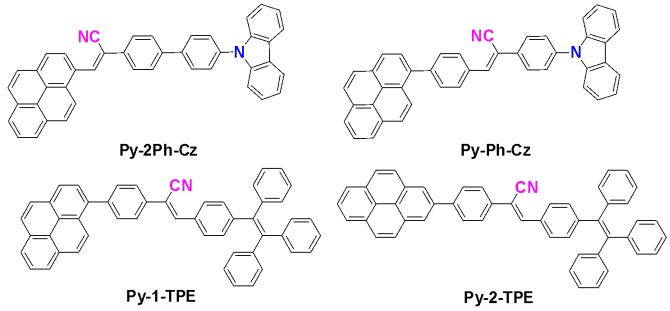

Figure 1. The synthesized target pyrene-based cyanostyrenes.

solvents, such as dichloromethane (DCM), tetrahydrofuran (THF) or toluene. Moreover, the twisted 3D molecular geometries of **Py-1-TPE** and **Py-2-TPE** exhibit better solubility than **Py-2Ph-Cz** and **Py-Ph-Cz**, which may be ascribed to the twist molecular structure of the bulky tetraphenylethylene unit hindering intramolecular interactions. As shown in Figure S23, the TGA results indicated that the compounds **Py-1-TPE** and **Py-2-TPE** displayed a slight weight loss (< 5%) over the range 25-220 °C, attributed to the water molecules in the lattice (the theoretic weight loss of H_2O is 2.64% for **Py-1-TPE,** and 2.01% for **Py-2-TPE**, respectively). It is noted that the endothermic band at around 233 °C with a weight loss of *ca*. 43 % corresponds to the fragment of phenylcarbazole in the molecular scaffold **Py-2Ph-Cz** being lost (the theoretic weight loss of phenylcarbazole in the compounds is 42.6%). The decomposition temperatures (T_d, 5% weight loss) of the four compounds are 189 °C, 430 °C, 466 °C and 459 °C, respectively.

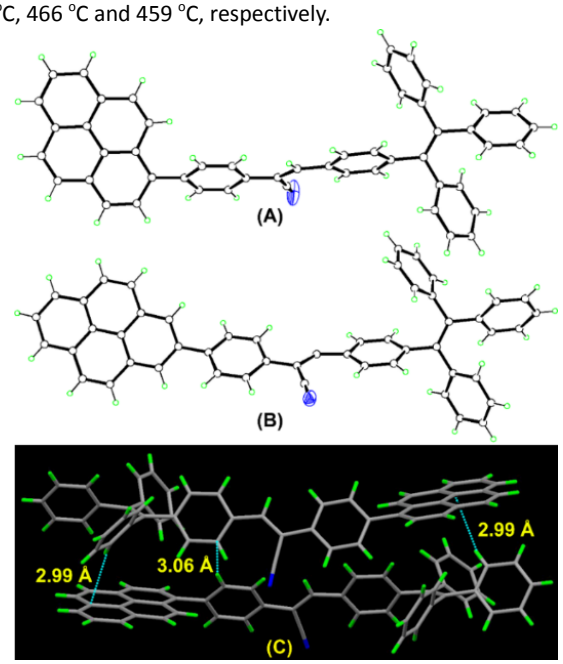

Figure 2. Single crystal structures of (A) **Py-1-TPE** and (B) **Py-2-TPE**, as ORTEP drawings with thermal ellipsoids at 30% probability. (C) The packing structure of **Py-1-TPE** showing the C-H···π interactions.

We attempt to cultivate suitable single crystals of the four pyrene-based cyanostyrene derivatives for X-ray crystallographic analysis, but only two suitable plate-like crystals, namely **Py-1-TPE** and **Py-2-TPE** were achieved *via* slow evaporation of a mixture of hexane and dichloromethane (V_{Hexane}:V_{DCM} = 1:1) at room temperature. The key crystallographic data and refinement parameters are presented in Table S1.

The crystal lattices of both **Py-1-TPE** and **Py-2-TPE** are centrosymmetric with the monoclinic space groups C 1 2/c 1. As shown in Figure 2, the pyrene and tetraphenylethylene units are separated by a cyanostyrene unit in the two crystals, which possess a unique non-planar geometry between the pyrene unit and the adjacent phenyl ring (at the 1- or 2-position of pyrene) with a dihedral angle of 52.92° for **Py-1-TPE** and 34.66° for **Py-1-TPE**, respectively. Although there are substituents at different positions of the pyrene (the 1- or 2-position), it is noteworthy that both compounds adopted almost identical molecular packing (head-to-tail manner) via several C-H···π interactions (Figure 2(C) and Figure S25-S27) in the crystalline state. Moreover, both crystals have trapped disorder water molecules in the void channels. No significant π···π interactions are observed in the packing of either

tetraphenylethylene unit.

Photophysical Properties

The UV-vis spectra of the four pyrene-based cyanostyrene derivatives in THF solution (10^{-5} M) are illustrated in Figure 3A. The compounds **Py-2Ph-Cz** and **Py-Ph-Cz** display two strong absorption bands in the range 275-300 nm and 320-425 nm, and the maximum absorption peak of **Py-2Ph-Cz** is red-shifted by 26nm compared to **Py-Ph-Cz**. This may be ascribed to extension of the π conjugation of the molecular skeletons. Compared to the 4-position substituted pyrene-based cyanostyrene ($\lambda_{max\ abs}$ = 327 nm),[39] the absorption spectra of **Py-Ph-Cz** still exhibits a red-shifted absorption band at 358 nm, which may be due to the substituent effect at the 1-position of pyrene.[55] Theoretically, the substituents at the 1-positions of pyrene exhibit strong electronic communication, whilst weak electronic communication occurs at the 2-position, this is because the nodal plane of pyrene passes through the C2 and C7 atoms,[55] and the difference in the electronic structure of pyrene would result in distinguishable electronic transitions. In this case, **Py-2-TPE** exhibits a pyrene-like absorption band at around 320-340 nm with a broad absorption peak at 377 nm, whilst for **Py-1-TPE**, with the substituent at the 1-position of the pyrene, the absorption peak at the long wavelength (377 nm) is the same as that for **Py-2-TPE,** however the molar absorption coefficient of **Py-1-TPE** (48425 M^{-1} cm^{-1}) is higher than **Py-2-TPE** (31392 M^{-1} cm^{-1}) (Table 1), which indicates that the 1-substituted pyrene strengthens the $S_1 \leftarrow S_0$ transitions, but weakens the $S_2 \leftarrow S_0$ transitions. In contrast, the 2-substituted pyrene exerts a large influence on the $S_2 \leftarrow S_0$ transitions, which is in good agreement with Marder's report. [55] In addition, the compound **Py-Ph-Cz** exhibited a relatively large molar absorption coefficient compared to **Py-2Ph-Cz** in the range 275-300 nm, which is consistent with the $S_3 \leftarrow S_0$ transitions. Thus, the results of this experience of molecular design can aid the construction of novel high-performance pyrene-based luminescent materials.

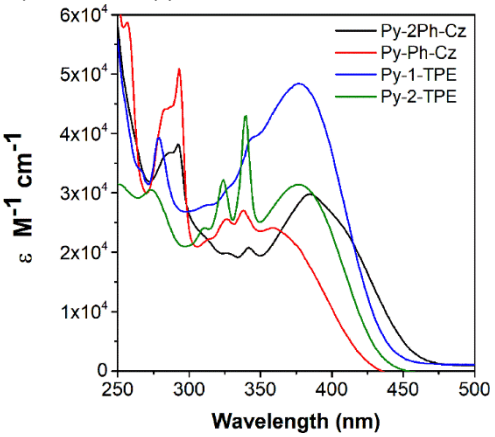

Figure 3. UV-vis spectra of four pyrene-based cyanostyrene derivatives in THF solution (10^{-5} M).

Previously, our group reported that the 4-substituted cyanostyrene pyrene derivatives were AIE-active materials.[39] In order to further explore the AIE properties of the four pyrene-based cyanostyrenes, the emission spectra (10^{-5} M) were measured in THF (good solvent) and THF/water (poor solvent) mixtures. Taking **Py-2Ph-Cz** as an example (Figure 4A and 4D), the emission maxima of **Py-2Ph-Cz** was located at 488 nm in pure THF solution, and as the water fraction (f_w) increased from 0% to 60%, the emission red-shifted to 498 nm with a weak blue fluorescence. Subsequently, the emission intensity rapidly enhanced with a larger red-shifted emission at 548 nm when the f_w increased to 90%, due to molecular aggregation. Furthermore, the formation of the molecular aggregation at f_w = 99% would slightly quench the fluorescence intensity of the maximum emission peak at 545 nm.

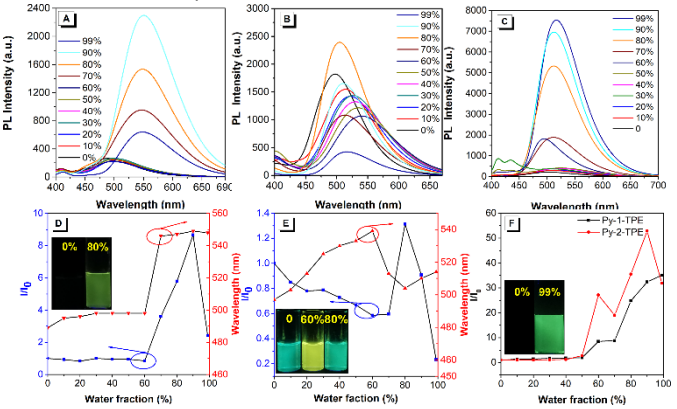

Figure 4. PL spectra of (A) **Py-2Ph-Cz**, (B) **Py-Ph-Cz** and (C) **Py-1-TPE** in THF/water mixtures with different water fractions (f_w). Plot of relative PL intensity (I/I_0) *versus* the composition of a THF/water mixture of (D) **Py-2Ph-Cz** (E) **Py-Ph-Cz** and (F) **Py-1-TPE** and **Py-2-TPE**, respectively. Inset: fluorescent photographs of **Py-2Ph-Cz** in THF/water mixtures (f_w = 0% and 80%), **Py-Ph-Cz** in THF/water mixtures (f_w = 0%, 60% and 80%) and **Py-1-TPE** in THF/water mixtures (f_w = 0% and 99%) taken under UV irradiation (λ_{ex} = 365 nm), where I_0 is the PL intensity in pure THF solution. The blue squares are for the effect on I/I_0, while red circles are for the wavelength.

Table 1. The photophysical properties of four pyrene-based cyanostyrene derivatives.

Compd	ε ($\lambda_{max\ abs}$) (M^{-1} cm^{-1}) [a]	λ_{maxPL} (nm) solns[a]/ films[b]	Φ_f solns[a]/ films[b]	τ (ns) solns[a]/ films[b]	α_{AIE} [c]	K_r (×10^8 S^{-1})[d] solns[a]/ films[b]	K_{nr} (×10^8 S^{-1})[e] solns[a]/ films[b]
Py-2Ph-Cz	2.98×10^4 (384)	488 / 547	0.01/0.08	0.20/2.49	8	0.50 / 0.32	49.50 / 3.69
Py-Ph-Cz	2.41×10^4 (358)	497 / 514	0.30/0.36	1.23/2.63	1.2	2.44 / 1.37	5.69 / 2.43
Py-1-TPE	4.84×10^4 (377)	498 / 514	0.01/0.45	1.29/1.97	45	0.08 / 2.28 (0.17 / 2.68)[f]	7.67 / 2.79 (4.19 / 1.43)[f]
Py-2-TPE	3.14×10^4 (377)	438,496/ 498	0.01/0.39	1.16/2.34	39	0.08 / 1.67 (0.01 / 2.77)[f]	8.5 / 2.6 (657.21 / 0.02)[f]

radiative decay rate (Φ/τ). [e]k_{nr} = nonradiative decay rate (1/τ - k_r). [f] Calculated by BDF package.

On the other hand, the solvatochromic effect results indicated that the **Py-2Ph-Cz** exhibited a large red-shifted emission with the maximum emission peak shifting from 488 nm to 500 nm, as the solvent polarity was increased from cyclohexane (Cy) to DMSO (Figure S28), and this can be attributed to the ICT effect.[56-58] Thus, we speculate the maximum emission peak at 545 nm for **Py-2Ph-Cz** at f_w = 99% is originating from the synergistic effect of the excimer emission plus the ICT process.

In the **Py-Ph-Cz** case, as the f_w increased from 0% to 60%, the emission intensity gradually decreased with a red-shifted emission from 497 nm to 539 nm compared to that observed in pure THF solution. Then, when the f_w increased to 80%, the emission intensity enhanced again (Figure 4B and 4E). However, the fluorescence intensity decreased with an accompanied blue-shifted emission band at around 514 nm, which can be ascribed to the formation of molecular aggregates at f_w = 99%, resulting in a H-aggregation. As expected, the absolute PL quantum yield (Φ_f) of **Py-2Ph-Cz** and **Py-Ph-Cz** were measured at 0.01 and 0.30 in THF solution accompanied with 0.08 and 0.36 in the film (Table 1), respectively, indicating that **Py-2Ph-Cz** is AIE-active and **Py-Ph-Cz** is AIEE-active.

When the phenylcarbazole group is replaced by a tetraphenylethylene unit, both compounds **Py-1-TPE** and **Py-2-TPE** exhibited typical AIE characteristics. As shown in Figure 4C and 4F, both compounds showed fluorescence signals in THF solution, as following the enhancement of f_w from 10% to 50%, the fluorescence intensity slightly increased. On sequentially increasing the f_w = 90%, the emission intensity enhanced dramatically by *ca*. 35-fold compared with that in pure THF solution, with the maximum emission wavelength at 515 nm for **Py-1-TPE** and 514 nm for **Py-2-TPE**. The PL quantum yield increased from 0.01 in THF solution to 0.45 for **Py-1-TPE** and 0.39 for **Py-2-TPE** in films**.** Thus, both **Py-1-TPE** and **Py-2-TPE** are AIE-active materials. In addition, the emission of both **Py-1-TPE** and **Py-2-TPE** in thin film exhibited a slight red-shifted (< 16 nm) emission compared with in THF solution. Thismay be due to the presence of TPE units, which play a crucial role in inhibiting the π-π stacking in the aggregation state. Generally, TPE-based molecules are known to follow the RIM mechanism, and major changes between the solution and solid state mainly concern the k_{nr} which are strongly decreased by forced rigidification of the structure (and restriction of rotation/vibrations and mostly isomerization processes) while k_r are marginally increased. For the **Py-1-TPE** and **Py-2-TPE** cases, the k_r increased from 10^6 s^{-1} in solution to 10^8 s^{-1} in the film, while the k_{nr} decreased by *ca.* 3-fold in the film compared to that in solution (Table 1 and Figure S39). This may be attributed to the presence of the cyanostyrene and TPE moieties, the synergistic effect of the RIM and the lone pairs participating in the light emission processes.[59]

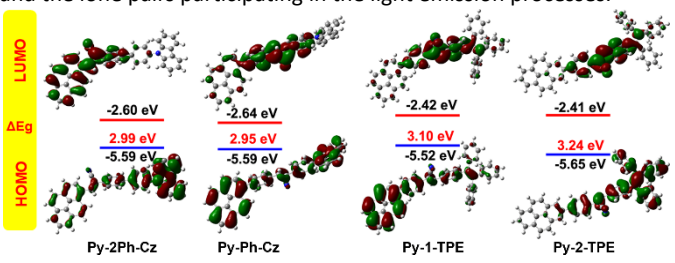

Figure 5. Molecular orbital plots of pyrene-based cyanostyrene AIEgens (from left to right: **Py-2Ph-Cz**, **Py-Ph-Cz**, **Py-1-TPE** and **Py-2-TPE**) calculated by the RB3LYP/6-311G(d,p) level.

Furthermore, density functional theory (DFT) calculations (B3LYP/6-311G (d,p)) on **Py-2Ph-Cz**, **Py-Ph-Cz**, **Py-1-TPE** and **Py-1-TPE** were performed to understand the effect of the electron delocalization on the optical behavior. The highest occupied molecular orbital (HOMO) and lowest unoccupied molecular orbital (LUMO) energy levels are charted in Figure 5. The HOMO of **Py-Ph-Cz** is almost completely delocalized over the entire molecule, whilst the HOMO of **Py-2Ph-Cz** is primarily distributed in the carbazole unit, and the HOMO of **Py-1-TPE** is localized on the pyrene unit and a portion of the the cyanostyrene unit**.** Given that the nodal plane of the pyrene passes through the carbon atoms at the 2,7-positions in the HOMO and LUMO, the substituents at the 2-positions will interact weakly with the pyrene core. Whereas when the substituents are at the 1-position, the electronic communication ability between the pyrene and the substituents would be increased. In our case, according to the DFT calculations, the pyrene mainly acts an electron donor in compounds Py-Ph-Cz, and Py-1-TPE, and in Py-2Ph-Cz, the pyrene unit was directly connected with the cyanostyrene fragment, which may acts a weak electron-withdrawing group. On the other hand, although the 2-position of pyrene was functionlized, this position has a limited effect on the electron structure of the whole molecule[55,60] The molecular orbital density in the HOMO of **Py-2-TPE** is localized on the tetraphenylethylene unit and the fragment of cyanostyrene. While the LUMO level of **Py-Ph-Cz, Py-1-TPE** and **Py-2-TPE** are distributed in the fragment of the cyanostyrene and partially on the tetraphenylethylene (phenylcarbazole) unit. For **Py-2Ph-Cz,** the LUMO is mainly spread on the pyrene ring and the cyanostyrene units. The separated HOMO and LUMO levels indicated that the pyrene-based cyanostyrene derivatives can undergo a twisted intramolecular charge transfer process in polar solvents, leading to an obvious red-shifted emission, as well as a decreased energy band gap.

In fact, the pyrene unit is an interesting chromophore, which can act as either an electron-donor or acceptor depending on the micro-environment of the bulk structure.[61] Thus, according to the DFT calculations, the pyrene may acts an electron-donating (D) or electron-withdrawing (A) group depending on the electronic properties of the peripheral substituent groups present. The carbazole and cyanostyrene fragments are regarded as electron-donating and electron-withdrawing group (A) respectively. Thus, the four pyrene-based cyanostyrene derivatives can be regarded as D-A type molecules. Indeed, the fluorescence spectra of the four compounds displayed a significant bathochromic shift as the solvent polarity increased from cyclohexane to dimethyl sulfoxide (DMSO) (Figure S28-31). Notably, large Stokes shifts of over 50 nm were observed, which further confirmed that the pyrene-based cyanostyrene with a D-A molecular structure can undergo a typical ICT transition, where the highly polar excited state is stabilized by polar solvents.[56] This result is consistent with their optical behavior.

Mechanochromic properties

Generally, the cyanostyrene derivatives with AIE characteristic prefer to exhibit mechanoluminescence/mechanochromism (ML/MC) properties under mechanical stimuli, which mainly originates from the molecular packing patterns or changing molecular configuration.[62] To test the MC properties of the twisted pyrene-based cyanostyrenes, the solid-state emission behavior was investigated before and after grinding. Compound **Py-Ph-Cz** exhibited an intense green emission (518 nm) in the crystalline state, after grinding, the crystalline structure easily crashed and the powder emitted a maximum emission peak at 512 nm, *i.e*. a slight hypsochromic shift in the fluorescence spectra (Figure 6A and 6B). For **Py-2Ph-Cz**, the maximum emission wavelength changed slightly

noteworthy that the maximum emission peak of both crystals **Py-1-TPE** and **Py-2-TPE** exhibited a red-shift from 494 nm to 512 nm after grinding (Figure 7 and Figure S38B). Clearly, the TPE-containing pyrene-based cyanostyrenes **Py-1-TPE** and **Py-2-TPE** revealed an obvious contrast of emission before and after grinding compared to **Py-Ph-Cz** and **Py-2Ph-Cz**. This can be attributed to the former TPE-containing compounds with the larger twist conformation becoming more planar.[39]

Furthermore, powder X-ray diffraction (PXRD) was utilized to determine the molecular pattern before and after grinding (Figure 6C-6D and Figure S40). The powdered samples of compounds **Py-2Ph-Cz, Py-Ph-Cz** and **Py-1-TPE** displayed a sharp and intense diffraction pattern before grinding, where the PXRD peak in region $2\theta = 20^{\circ}$-30° is tentatively assigned to π-π stacking interactions in the range 3.1-4.40 Å.[39,63] However, after grinding, the PXRD pattern of **Py-2Ph-Cz, Py-Ph-Cz** is the same as their crystalline PXRD pattern with a decreased reflection intensity and broadened FWHM, which indicates that the crystal unit cell remains unchanged after grinding. For **Py-1-TPE**, the diffraction peaks at $2\theta = 22.0^{\circ}$ disappeared with a new peak appearing at $2\theta = 38.2^{\circ}$, which revealed that the external forces can strengthen the intermolecular interactions, such as C-H···π interactions.

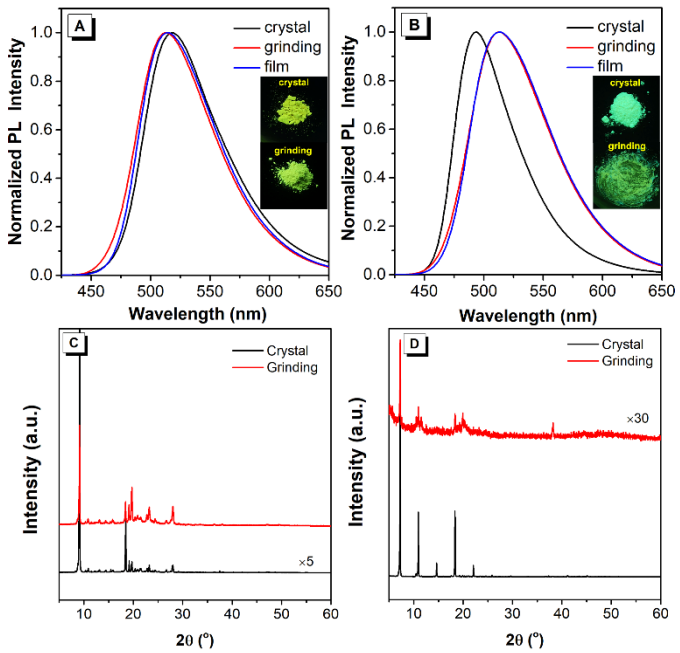

Figure 6. The PL spectrum of (A) **Py-Ph-Cz** and (B) **Py-1-TPE** before and after grinding, Inset: the images of compounds in the crystalline state and after grinding taken under 365 nm UV light. Wide angle XRD diffractograms of (C) **Py-Ph-Cz** and (D) **Py-1-TPE** in different states.

Preparation of pyrene-based AIEgens fluorescent ink for patterning

Before utilizing these systems for printing ink, the cytotoxicity was evaluated using a 3-(4,5-dimethyl-2-thiazolyl)-2,5-diphenyltetrazolium bromide (MTT) assay. As shown in Figure S41, the NCTC clone 929 [L cell, L-929] cell viability remains close to 100% as the concentration of the four compounds increased from 0 to 50μM after 24h of incubation. This indicated that the pyrene-based AIEgens exhibited low toxicity to the normal live cells. Thus, cell survival experiments results indicated that the pyrene-based AIEgens would be suitable luminescent materials to be used as fluorescence inks for industrial applications.

properties, and good biocompatibility, a new fluorescence ink was fabricated using the pyrene-based AIEgens as the luminescent material.[64] The selected AIEgens powders (**Py-2Ph-Cz**, **Py-Ph-Cz** and **Py-1-TPE**, **Py-2-TPE** were not tested due to their similar photophysical features to **Py-1-TPE**) were dissolved in epoxy resin (100g) to achieve a colorless or pale yellow fluorescence (depending on the concentration of pyrene-based AIEgens) ink under sunlight. The schematic on the anti-counterfeiting ink and screen-printing process is illustrated in Figure 7A. The three fluorescence inks exhibited bright blue or sky-blue emission in both resins (epoxy resin and polypropylene) solution. Moreover, the ink is stable even after prolonged standing (4 months) at room temperature.

Before printing, for the epoxy resin system, the curing agent (593 curing agent, 25 g) was added into the ink in order to solidify the epoxy resin. Then, as shown in Figure 7B and S42-43, the letters "AIE" were printed upon the filter paper, butter paper and tissue paper via screen printing technology using the pyrene-based AIEgens inks. As the content of the fluorescence powder increased from 1 mg to 5 mg, the high quality fluorescence patterns (such as high contrast, distinguishable outlines) became clearer with good printability on the three types of papers. When the weight ratio of the pyrene-based AIEgens:(epoxy resin+ curing agent) reached *ca.* 5:125,000 (0.004 wt%), the emission intensity was enhanced by *ca.* 1-4 fold and with clear "AIE" images observed (Figure S51-54).

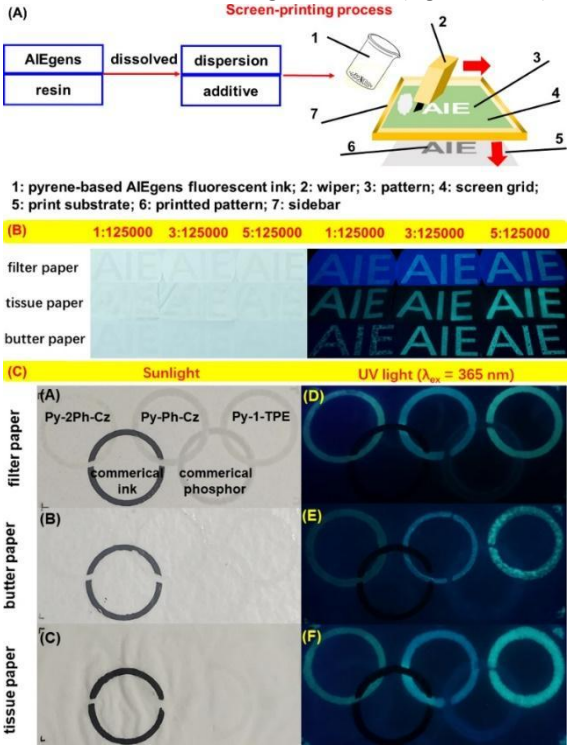

Figure 7. **(**A) The schematic on the anti-counterfeiting ink and screen-printing process (B) Digital photographs of letter "AIE" pattern printing on filter paper, butter paper and tissue paper using pyrene-based AIEgens **Py-1-TPE** as fluorescence ink with different concentration ($Weight_{AIEgens}$:$Weight_{Epoxylite+curing\ agent}$ = 1:125000, 3:125000 and 5:125000) under sunlight (Left) and UV irradiation (λ_{ex} = 365 nm) (Right), (C) Digital photographs of Olympic ring pattern printing on (left) filter paper, butter paper and tissue paper using pyrene-based AIEgens fluorescence ink or commercial ink ($Weight_{AIEgens\ or\ inorganic\ phosphor}$:$Weight_{Epoxylite+curing\ agent}$ = 5:125000) under sunlight, (right) under UV irradiation (λ_{ex} = 365 nm). (under UV irradiation: Aperture: f/1.8, Exposure time: 1/40s, ISO speed: ISO-400).

of the olympic rings was overprinting using **Py-2Ph-Cz**, **Py-Ph-Cz** and **Py-1-TPE** as the fluorescence ink, respectively. For comparison, the common commercial black ink (fluorescent material free), commercial inorganic phosphor ($BaMgAl_{11}O_{19}$ $Ce^{3+}Tb^{3+}$, Φ_f = 0.90), RhodamineB (RhB) and fluorescein (both are selected as commercial red/yellow fluorescent dyes with ACQ feature) were also selected. As shown in Figure 7C, the fluorescent inks show an almost invisible profile on the butter paper and tissue paper, but a shallow imprinting on the filter paper in sunlight. Upon irradiation (λ_{ex} = 365 nm), the clear figures of three rings for the pyrene-based AIEgens appeared, while the commercial inorganic phosphor did not exhibit a visible pattern, because of its ultralow concentration in the fluorescent ink. Only when the weight ratio was increased to 5:32, did the commercial inorganic phosphor display a visible image (Figure S44) under λ_{ex} = 256 nm irradiation. Also, the letters "AIE" were printing on the wall with bright emission under UV irradiation in the dark (Movies S1).

On the other hand, one of the greatest challenges when employing organic fluorescence ink is how to avoid or minimize color migration of the fluorescent pattern, which is related to the quality of the printing products. As shown in Figures S42-S43, Figure S45, and Table S5, the fluorescent ink containing pyrene-based AIEgens (0.004 wt%) has a relatively small color migration (< 27 nm) in butter paper and tissue paper substrate compared to their powders in solid state. In contrast, the fluorescence ink containing RhB or fluorescein also showed a clear fluorescent pattern with a maximum blue shifted emission of 140 nm at ultralow concentration in the three print substrates compared to the pure compound in the solid state (Figures S46-S47). The large blue-shift may be ascribed to the fluorescent dyes with an ACQ feature reacting with the curing agent.

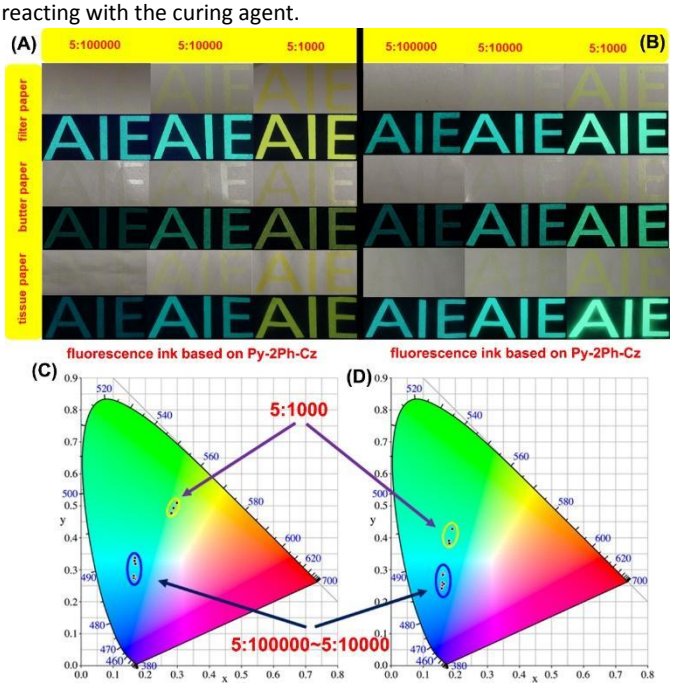

Figure 8. Digital photographs of the letters "AIE" pattern printing on filter paper, butter paper and tissue paper using pyrene-based AIEgens **Py-2Ph-Cz** (A) and **Py-1-TPE** (B) as fluorescence ink at different concentrations ($Weight_{AIEgens}$:$Weight_{pp}$ = 5:100000, 5:10000 and 5:1000, respectively) under sunlight and UV irradiation of 365 nm (B, D, and F). (under UV irradiation: Aperture: f/1.8, Exposure time: 1/40s, ISO speed: ISO-400), (C) and (D) CIE 1931 chromaticity diagram. the color coordinates for the corresponding concentration.

preparing the fluorescence ink which easily solidified by evaporation at room temperature. The effect of concentration on the color migration was investigated using **Py-2Ph-Cz, Py-1-TPE,** RhB and fluorescein as fluorescent dyes in the polypropylene system. For example, the fluorescent ink containing **Py-2Ph-Cz** revealed a clear security pattern with similar emission color from $Weight_{AIEgens}$:$Weight_{pp}$ = 5:100000 to 5:10000 (0.005 wt% to 0.05 wt%) with small color migration (9 nm) in the three printing substrates, and this was almost imperceptible by naked-eye detection. When the concentration increased to 0.5 wt%, the maximum emission band was red-shifted to *ca*.530 nm, which corresponded to its emission peak (547 nm) in the aggregate state (Figure 8A and Figure S56). In the **Py-1-TPE** case, the fluorescent inks exhibited similar emission behavior ($\lambda_{max\ em}$: 472-492 nm) with slight color migration (17 nm) in three substrates as the concentration increased *ca*. 100-fold from $Weight_{AIEgens}$:$Weight_{pp}$ = 5:100000 to 5:1000 (0.005 to 0.5 wt%). More importantly, the higher the concentration of the content of AIEgens in the PP resin, brighter emissive was observed (Figure 8B and Figure S55-S56). However, in the fluorescein and RhB systems, as the concentration increased from 0.005 to 0.5 wt%, both fluorescence inks exhibited dual emissive fluorescent behavior with tunable-color emission from a blue to yellow-green color for fluorescein, and a white to orange-red color for RhB. Moreover, the emission intensity suffered somewhat from fluorescent quenching at high concentration of fluorescein (0.5 wt%) compared to 0.05 wt% concentration (Figure S48-S49 and Figure S57-S58).

Based on our previous knowledge and the experimental results, traditional fluorescent inks contain organic dyes (such as RhB, fluorescein etc.) and prefer to undergo an uncontrollable color migration, leading to a concentration-dependant emission color in the fluorescence ink, and the inorganic fluorescence ink has a large amount content of inorganic phosphor. More importantly, both of the inorganic fluorescence materials and the commercial organic dyes would cause the fluorescence intensity to decrease due to the ACQ effect in high concentration. However, the AIE materials are molecularly dispersed in a matrix and the RIM mechanism still works. The fluorescent inks containing a low concentration of pyrene-based AIEgens show some advantages, namely (I) a wide scope of application over the range from ultralow to low concentration (0.005-0.5 wt%) to avoid the ACQ effect, (II) good biocompatibility with impressive anti-counterfeiting features, and (III) slight color migration, which not only offers an example of the use of AIEgens as anti-counterfeiting inks with ultralow consumption for commercial application, but also enriches the practical applications of AIEgens.

Experimental

Materials:

Unless otherwise stated, all reagents used were purchased from commercial sources and were used without further purification. Tetrahydrofuran was distilled prior to use.

Characterization

^1H and ^{13}C NMR spectra (400 MHz or 600MHz) were recorded on a Bruker AV 400M or AVANCE III 600M spectrometer using chloroform-*d* solvent and tetramethylsilane as internal reference. *J*-values are given in Hz. High-resolution mass spectra (HRMS) were taken on a LC/MS/MS, which consisted of a HPLC system (Ultimate 3000 RSLC, Thermo Scientific, USA) and a Q Exactive Orbitrap mass spectrometer. UV-vis absorption spectra and photoluminescence (PL) spectra were recorded on a Shimadzu UV-2600 and the Hitachi F-4700 spectrofluorometer. PL quantum yields were measured using

Analyzer. The lifetime was recorded on an Edinburgh FLS 980 instrument and measured using a time-correlated single-photon counting method. Thermogravimetric analysis was carried on a Mettler ToledoTGA/DSC3+ under dry nitrogen at a heating rate of 10 °C/min. The quantum chemistry calculation was performed on the Gaussian 09 (B3LYP/6–311G (d,p) basis set) software package. The solid environment was simulated by two-layer ONIOM model with QM/MM method, and the simulated rates of radiative/nonradiative decay were calculated by Molecular Material Property Prediction Package (MOMAP).

X-ray Crystallography

Crystallographic data for the compounds was collected on a Bruker APEX 2 CCD diffractometer with graphite monochromated Mo Kα radiation (λ = 0.71073 Å) in the ω scan mode. [65,66] The structures were solved by charge flipping or direct methods algorithms and refined by full-matrix least-squares methods on F^2.[67] All esds (except the esd in the dihedral angle between two l.s. planes) were estimated using the full covariance matrix. The cell esds were considered individually in the estimation of esds in distances, angles and torsion angles. Correlations between esds in cell parameters were only used when they were defined by crystal symmetry. An approximate (isotropic) treatment of cell esds was used for estimating esds involving l.s. planes. The final cell constants were determined through global refinement of the xyz centroids of the reflections harvested from the entire data set. Structure solution and refinements were carried out using the SHELXTL-PLUS software package.[67] The partially occupied water molecule of crystallization was modelled by the Platon Squeeze procedure.[68] Data (excluding structure factors) on the structures reported here have been deposited with the Cambridge Crystallographic Data Centre. CCDC 2059788 and 2059789 contains the supplementary crystallographic data for this paper. These data could be obtained free of charge from The Cambridge Crystallographic Data Centre via www.ccdc.cam.ac.uk/data_request/cif.

Cell viability

L929 mouse fibroblasts were cultured in Dulbecco's modified eagle medium (DMEM) containing 10% fetal bovine serum at 37 °C in a humidified environment containing 5% CO_2. The cytotoxicity of compounds **Py-2Ph-Cz**, **Py-Ph-Cz**, **Py-1-TPE**, **Py-2-TPE** and pyrene were assessed by the 3-(4,5-dimethylthiazol-2-y1)-2,5-diphenyltetrazolium bromide (MTT) method. L929 mouse fibroblasts were firstly seeded into a 96-well plate at a density of 8000 cells per well in DMEM, and incubated for 24 h. Then the media were replaced by the different concentrations (0, 0.78, 1.56, 3.12, 6.25, 12.5, and 25 μg/mL) of pyrene and (1.56, 3.13, 6.25, 12.5, 25, and 50 μg/mL) of pyrene-based AIEgens, and cells were incubated for another 24 h. After incubation, the culture media were removed and each well was filled with 100 μL of new culture media containing MTT (0.5 mg/mL) and incubation for additional 4 h. Then the media was discarded and each well was added with another 100 μL DMSO. The OD490 value (Abs.) of each well was measured by microplate reader immediately. Cell viability was calculated by the ratio of OD490 values of the cells incubated with five compound suspension to that of the cells incubated with culture medium only.

The screen-printing procedure

For the epoxy resin system fluorescence ink: An amount of fluorescence powder (**Py-2Ph-Cz**, **Py-Ph-Cz**, **Py-1-TPE,** RhB or commercial phosphor $BaMgAl_{11}O_{19}$ $Ce^{3+}Tb^{3+}$) (1mg, 3 mg and 5 mg) was added in epoxy resin (100 g) and stirred for 1 h to ensure uniform fluorescence dispersion. Before printing, the curing agent (25 g) was added into the fluorescence ink system for controlling the curing time. Then the anti-counterfeiting images were fabricated using the common screen-printing technology.

For the polypropylene system fluorescence ink: An amount of fluorescence powder (**Py-2Ph-Cz**, **Py-Ph-Cz**, **Py-1-TPE,** RhB or fluorescein) was added to polypropylene (100 g) and stirred for 1 h to ensure uniform fluorescence dispersion. Then the prepared anti-counterfeiting images were fabricated using the common screen-printing technology.

Synthetic procedures

The starting compounds 2-Bpin-Pyrene (**1c**)[60] or intermediates 2-(4'-(8a,9a-dihydro-9H-carbazol-9-yl)-[1,1'-biphenyl]-4-yl)acetonitrile (**2a**)[69], 1-(4-formylphenyl) pyrene (**2b**)[70], 2-(4-(pyren-1-yl)phenyl)acetonitrile (**2c**), 2-(4-(pyren-2-yl)phenyl)acetonitrile (**2d**) and (Z)-2-(4-bromophenyl)-3-(4-(pyren-1-yl)phenyl)acrylonitrile (**3a**) were synthesized and are listed in the Scheme S1.

General procedure for synthesis of (Z)-2-(4'-(9H-carbazol-9-yl)-[1,1'-biphenyl]-4-yl)-3-(pyren-1-yl) acrylonitrile (Py-2Ph-Cz)

To a 100mL two-necked flask was added 2-(4'-(9H-carbazol-9-yl)-[1,1'-biphenyl]-4-yl) acetonitrile (150 mg, 0.41 mmol, 1 eq.), 1-(4-formylphenyl) pyrene (113mg, 0.50mmol, 1.22 eq.), KO*t*Bu (150 mg, 1.34 mmol, 3.27 eq.) and dry ethanol (10 mL). The reaction mixture was degassed with nitrogen for 5 min., and the mixture was refluxed overnight at 90°C. After cooling to room temperature, the reaction mixture was filtered by washing with cold ethanol three times, then the residue was further crystallized from a mixture of hexane and dichloromethane to afford (Z)-2-(4'-(9H-carbazol-9-yl)-[1,1'-biphenyl]-4-yl)-3-(pyren-1-yl) acrylonitrile (**Py-2Ph-Cz**) as a yellow solid (320 mg, 74%) (In addition, the compound **Py-2Ph-Cz can** transfer from the trans-configuration to cis-configuration in the solvent slowly). ^{1}H NMR (400 MHz, $CDCl_3$): δ 8.71 (d, J = 8.2 Hz, 1H), 8.69 (s, 1H), 8.35 – 8.04 (m, 10H), 8.00 (d, J = 8.5 Hz, 2H), 7.94 – 7.89 (m, 2H), 7.87 (d, J = 8.6 Hz, 2H), 7.77 – 7.68 (m, 2H), 7.52 (d, J = 8.2 Hz, 2H), 7.49 – 7.43 (m, 2H), 7.38 – 7.29 (m, 2H) ppm. ^{13}C NMR (101 MHz, $CDCl_3$) δ 141.3, 140.8, 140.2, 139.0, 137.5, 133.9, 133.0, 131.3, 130.7, 123.0, 128.9, 128.5, 127.9, 127.8, 127.5, 126.8, 126.4, 126.3, 126.2, 126.1, 126.0, 125.1, 124.8, 124.6, 123.5, 122.6, 120.4, 120.1, 118.2, 114.3, 109.8 ppm. HRMS (FTMS+p APCI) m/z: found, 570.2116[M]$^+$; calcd for $C_{43}H_{26}N_2$ requires [M]$^+$ 570.2096.

General procedure for synthesis of (Z)-2-(4-(9H- carbazole-9-yl) phenyl-3-(4-(pyren-1-yl)phenyl)acrylonitrile (Py-Ph-Cz)

Under a nitrogen atmosphere, a mixture of (Z)-2-(4-bromophenyl)-3-(4-(pyren-1-yl)phenyl)acrylonitrile (220 mg, 0.45 mmol, 1.0 eq.), carbazole (91 mg, 0.54 mmol, 1.2 eq.) and K_2CO_3 (300 mg, 2.18 mmol, 4.84 eq.) were dissolved in a mixture of P(*t*Bu)$_3$ (1ml)/ toluene (8 mL). After degassing with nitrogen for 5 min., $Pd(OAc)_2$ (50 mg, 0.22 mmol, 0.48 eq.) was added, and the mixture was refluxed for 2 days at 110°C. After cooling to room temperature, the mixture was poured into H_2O (100 mL) and extracted with CH_2Cl_2 (3 × 50 mL). The combined organic layer was washed with water and brine (50 mL), and then the solution was dried over $MgSO_4$ and evaporated. The crude product was further purified by column chromatography using hexane/dichloromethane (V_{hexane}:V_{CH2Cl2} = 1:1) as the eluent which eventually afforded the yellow solid **Py-Ph-Cz** (105 mg, 40%). (In addition, the compound **Py-Ph-Cz** can transfer from the trans-configuration to cis-configuration in the solvent within 60 min. (Figure S12)) ^{1}H NMR (400 MHz, $CDCl_3$) δ 8.31 – 7.97 (m, 15H), 7.82 (s, 3H), 7.79 (d, *J* = 4.7 Hz, 2H), 7.73 (d, *J* = 8.4 Hz, 2H), 7.54 – 7.42 (m, 4H), 7.34 (t, *J* = 7.3 Hz, 2H) ppm. ^{13}C NMR (151 MHz, $CDCl_3$) δ 144.4, 144.0, 143.3, 142.2, 140.6, 140.4, 138.8, 138.7, 136.4, 136.2, 133.4, 132.5, 132.3, 131.6, 131.5, 131.3, 131.1, 131.0, 130.98, 131.0, 130.6, 123.0, 129.5, 128.5, 128.3, 128.0, 127.8, 127.6, 127.5, 127.4, 126.2, 126.2, 125.5, 125.1, 125.1, 125.0, 124.9, 124.8, 124.8, 124.8, 124.7 123.7, 120.5, 120.4, 120.4, 120.1, 118.1, 113.5, 110.8, 109.8, 109.7, 77.3, 77.0,

$C_{43}H_{26}N_2$ requires $[M]^+$ 570.2096.

General procedure for synthesis of (Z)-2-(4-(pyren-1-yl)phenyl)-3-(4-(1,2,2-triphenylvinyl)phenyl)acrylonitrile (Py-1- TPE)

Under a nitrogen atmosphere, a mixture of **2c** (100 mg, 0.315 mmol, 1 eq.), 4-(1,2,2-triphenylethenyl) benzaldehyde (124 mg, 0.35 mmol, 1.1 eq.) and KO*t*Bu (100 mg, 0.89 mmol, 2.83 eq.) in dry ethanol (6 mL) was refluxed overnight at 90°C. After cooling to room temperature, the reaction mixture was filtered and washed with cold ethanol three times, then the residue was further crystallized from a mixture solution of hexane and dichloromethane to give a yellow-green powder **Py-1-TPE**（103 mg, 50%). ^{1}H NMR (400 MHz, $CDCl_3$) δ 8.29 – 8.14 (m, 4H), 8.12 (s, 2H), 8.09 – 7.95 (m, 3H), 7.84 (d, *J* = 8.3 Hz, 2H), 7.72 (dd, *J* = 8.3, 6.5 Hz,4H), 7.55 (s, 1H), 7.22 – 6.99 (m, 17H) ppm. ^{13}C NMR (151 MHz, $CDCl_3$) δ 146.6, 143.4, 143.3, 143.2, 142.4, 142.1, 141.9, 140.0, 136.5, 133.7, 132.0, 131.7, 131.5, 131.4, 131.4, 131.3, 131.3 130.9, 130.9, 128.9, 128.5, 127.9, 127.9, 127.8, 127.7, 127.4, 127.4, 126.9, 126.8, 126.7, 126.1, 125.9, 125.3, 125.0, 125.0, 124.9, 124.9, 124.7, 118.2, 110.3 ppm. HRMS (FTMS+p APCI) m/z: found, 660.2687 $[M+H]^+$; calcd for $C_{51}H_{33}N$ requires $[M]^+$ 659.2613.

General procedure for synthesis of (Z)-2-(4-(pyren-2-yl)phenyl)-3-(4-(1,2,2-triphenylvinyl)phenyl)acrylonitrile (Py-2-TPE)

Under a nitrogen atmosphere, a mixture of **2d** (80 mg, 0.252 mmol, 1 eq.), 4-(1,2,2-triphenylethenyl) benzaldehyde (100 mg, 0.277 mmol, 1.1 eq.) and KO*t*Bu (80 mg, 0.71 mmol, 2.8 eq.) in dry ethanol (8 mL) was refluxed overnight at 90°C. After cooling to room temperature, the reaction mixture was filtered and washed with cold ethanol three times, then the residue was further crystallized from a mixture solution of hexane and dichloromethane to give a yellow-green powder **Py-2-TPE** (58 mg, 35 %). ^{1}H NMR (400 MHz, $CDCl_3$) δ 8.41 (s, 2H), 8.21 (d, *J* = 7.6 Hz, 2H), 8.17 – 8.09 (m, 4H), 8.06 – 7.99 (m, 2H), 7.96 (d, *J* = 8.4 Hz, 2H), 7.96 (d, *J* = 8.4 Hz, 2H), 7.82 (d, *J* = 8.4 Hz, 2H), 7.72 (d, *J* = 8.4 Hz, 2H), 7.52 (d, *J* = 3.2 Hz, 2H), 7.10 (m, 17H) ppm, ^{13}C NMR (151 MHz, $CDCl_3$) δ 146.6, 143.4, 143.3, 143.2, 142.4, 142.2, 141.7, 140.1, 137.6, 133.8, 132.0, 131.7, 131.4, 131.4, 131.3, 131.2, 128.9, 128.6, 128.0, 127.9, 127.9, 127.7, 127.5, 126.9, 126.8, 126.5, 126.1, 125.3, 124.5, 124.2, 123.5, 118.2, 110.2 ppm. HRMS (FTMS+p APCI) m/z: found, 660.2690 $[M+H]^+$; calcd for $C_{51}H_{33}N$ requires $[M]^+$ 659.2613.

Conclusions

In summary, a series of pyrene-based AIEgens were synthesized by a Knoevenagel reaction and a Pd-catalyzed coupling reaction in high yield. Together with their high thermal stability, excellent fluorescence properties, good biocompatibility, and light stability, the pyrene-based AIEgens were employed in the preparation of fluorescence inks for anti-counterfeiting by screen-printing technology. More importantly, the fluorescence ink containings compound **Py-1-TPE** with the TPE unit exhibited a more better printability on different substrates with small color migration at ultralow/low concentration (WeightAIEgens:Weightbinder = 0.005 ~0.5 wt%). Thus, such a fluorescence ink containing the pyrene-based AIEgens is a promising candidate for anti-counterfeiting applications and has the potential to significantly lower the costs with limited color migration involved in this industry. Ongoing work is focused on more color-tunable pyrene-based AIEgens from blue to red fluorescence inks.

Author Contributions

designing and performing the whole project and write paper; Z. Mu, L. An, W. Zhang, C. Cao and C. Redshaw contribution in revising the manuscript and giving scientific advice; X. Feng, A. Qin and B. Z. Tang contribution in designing and supervising the whole project.

Conflicts of interest

There are no conflicts to declare.

Acknowledgements

This work was supported by the National Natural Science Foundation of China (21975054 and 21905028), Natural Science Foundation of Guangdong Province of China (2019A1515010925), Guangdong Provincial Key Laboratory of Information Photonics Technology (2020B121201011), Guangdong Province Training Program of Innovation and Entrepreneurship for Undergraduates, “One Hundred Talents Program” of the Guangdong University of Technology (GDUT) (1108-220413205), Guangdong provincial key laboratory of functional soft condensed matter of the Guangdong University of Technology (GDUT) (220413205). CR thanks the EPSRC for an Overseas Travel Grant (EP/R023816/1). Thanks to Dr.Jianyu Zhang (HKUST) for the theoretical calculations.

Notes and references

1 https://www.worldtrademarkreview.com/economic-impact-counterfeiting-strategies-secure-sustainability.
2 F. Schneider, *Public Finance Review*, 2013, **41**, 677-707.
3 OECD, The Economic Impact of Counterfeiting and Piracy, OECD Publishing, Paris, 2008.
4 P. Kumar, S. Singh and B. K. Gupta, *Nanoscale*, 2016, **8**, 14297-14340.
5 Z. Long, Y. Wen, J. Zhou, J. Qiu, H. Wu, X. Xu, X. Yu, D. Zhou, J. Yu and Q. Wang, *Advanced Optical Materials*, 2019, **7**, 1900006.
6 B. Duong, H. Liu, C. Li, W. Deng, L. Ma and M. Su, *ACS Appl. Mater. Interfaces*, 2014, **6**, 8909.
7 L. Xu, J. Chen, J. Song, J. Li, J. Xue, Y. Dong, B. Cai, Q. Shan, B. Han and H. Zeng, *ACS Appl. Mater. Interfaces*, 2017, **9**, 26556-26564.
8 N. Waiskopf, S. Magdassi and U. Banin, *J. Am. Chem. Soc.*, 2021, **143**, 577.
9 G. Gao, D. Busko, R. Joseph, I. A. Howard, A. Turshatov and B. S. Richards, *ACS Appl. Mater. Interfaces*, 2018, **10**, 39851.
10 J. F. Mei, Z. P. Lv, J. C. Lai, X. Y. Jia, C. H. Li, J. L. Zuo and X. Z. You, *Dalton Trans.*, 2016, **45**, 5451-5454.
11 S. Qu, X. Wang, Q. Lu, X. Liu and L. Wang, *Angew. Chem. Int. Ed.*, 2012, **51**, 12215.
12 S. Kalytchuk, Y. Wang, K. Polakova and R. Zboril, *ACS Appl. Mater. Interfaces*, 2018, **10**, 29902.
13 J. Guo, H. Li, L. Ling, G. Li, R. Cheng, X. Lu, A.-Q. Xie, Q. Li, C.-F. Wang and S. Chen, *ACS Sustainable Chem. Eng.,* 2019, **8**, 1566.
14 Q. Dai, Q. Yu, Y. Tian, X. Xie, A. Song, F. Caruso, J. Hao and J. Cui, *ACS Appl. Mater. Interfaces*, 2019, **11**, 29305.
15 X. He, Y. Gu, B. Yu, Z. Liu, K. Zhu, N. Wu, X. Zhao, Y. Wei, J. Zhou and Y. Song, *J. Mater.Chem. C*, 2019, **7**, 14069.
16 H. Yang, W. Zhao, E. Song, R. Yun, H. Huang, J. Song, J. Zhong, H. Zhang, Z. Nie and Y. Li, *J. Mater.Chem. C*, 2020, **8**, 16533.
17 W. Yao, Q. Tian, J. Liu, Q. Xue, M. Li, L. Liu, Q. Lu and W. Wu, *Nanoscale*, 2017, **9**, 15982.
18 J. Xu, B. Zhang, L. Jia, Y. Fan, R. Chen, T. Zhu and B. Liu, *ACS Appl. Mater. Interfaces*, 2019, **11**, 35294.
19 X. Li, C. Yang, Y. Yu, Z. Li, J. Lin, X. Guan, Z. Zheng and D. Chen, *ACS Appl. Mater. Interfaces*, 2020, **12**, 18705.

Zhong, T. Supasai and Q. Zhang, *Langmuir*, 2018, **34**, 10363.
21 M. Zuo, W. Qian, T. Li, X. Y. Hu, J. Jiang and L. Wang, *ACS Appl. Mater. Interfaces*, 2018, **10**, 39214.
22 X. Han, F. Ge, J. Xu, X.-H. Bu, *Aggregate*, 2021, DOI: 10.1002/agt2.28.
23 Y. D. He, Z. L. Zhang, J. Xue, X. H. Wang, F. Song, X. L. Wang, L. L. Zhu and Y. Z. Wang, *ACS Appl. Mater. Interfaces*, 2018, **10**, 5805.
24 J. Mei, N. L. C. Leung, R. T. K. Kwok, J. W. Y. Lam and B. Z. Tang, *Chem. Rev.*, 2015, **115**, 11718.
25 J. Luo, Z. Xie, J. W. Lam, L. Cheng, H. Chen, C. Qiu, H. S. Kwok, X. Zhan, Y. Liu, D. Zhu and B. Z. Tang, *Chem. Commun.*, 2001, 1740.
26 J. Qu, X. Zhao, Y. Liang, T. Zhang, P. X. Ma and B. Guo, *Biomaterials*, 2018, **183**, 185.
27 C. McGregor, C. Perrin, M. Monck, P. Camilleri and A. J. Kirby, *J. Am. Chem. Soc.*, 2001, **123**, 6215.
28 H. Cao, Y. Yang, J. Li, *Aggregate*, **2020**, *1*, 69.
29 T. M. Figueira-Duarte and K. Mullen, *Chem. Rev.*, 2011, **111**, 7260.
30 J.-W. Oh, T. H. Kim, S. W. Yoo, Y. O. Lee, Y. Lee, H. Kim, J. Kim and J. S. Kim, *Sens. Actuators B Chem*., 2013, **177**, 813.
31 F. Wu, Y. Lu, X. Mu, Z. Chen, S. Liu, X. Zhou, S. Liu and Z. Li, *ACS Appl. Mater. Interfaces*, 2020, **12**, 32388.
32 M. S. Lone, S. Afzal, O. A. Chat, P. A. Bhat, R. Dutta, Y. Zhang, N. Kundu and A. A. Dar, *J. Phys. Chem. B*, 2019, **123**, 9699-9711.
33 Y. Pang, R. Zhao, Y. Lu, J. Liu, X. Dong and F. Xi, *New J. Chem.*, 2018, **42**, 17091.
34 L. Chen, B. Hu, J. Zhang, J. Zhang, S. Huang, P. Ren, Y. Zou, F. Ding, X. Liu and H. Li, *RSC Advances*, 2019, **9**, 476.
35 J.-M. Zhang, H.-B. Li, *Packing Engineering*, 2018, **39**, 104-111.
36 X. Feng, J. Y. Hu, C. Redshaw and T. Yamato, *Chem. Eur. J.,* 2016, **22**, 11898.
37 M. M. Islam, Z. Hu, Q. Wang, C. Redshaw and X. Feng, *Mater. Chem. Front.*, 2019, **3**, 762.
38 J. Yang, J. Huang, N. Sun, Q. Peng, Q. Li, D. Ma and Z. Li, *Chem. Eur. J.,* 2015, **21**, 6862.
39 X. Feng, J. Zhang, Z. Hu, Q. Wang, M. M. Islam, J.-S. Ni, M. R. J. Elsegood, J. W. Y. Lam, E. Zhou and B. Z. Tang, *J. Mater.Chem. C*, 2019, **7**, 6932.
40 X. Feng, C. Qi, H. T. Feng, Z. Zhao, H. H. Y. Sung, I. D. Williams, R. T. K. Kwok, J. W. Y. Lam, A. Qin and B. Z. Tang, *Chem. Sci.*, 2018, **9**, 5679.
41 J. Yang, L. Li, Y. Yu, Z. Ren, Q. Peng, S. Ye, Q. Li and Z. Li, *Mater. Chem. Front.*, 2017, **1**, 91.
42 X. Feng, Z. Xu, Z. Hu, C. Qi, D. Luo, X. Zhao, Z. Mu, C. Redshaw, J. W. Y. Lam, D. Ma and B. Z. Tang, *J. Mater.Chem. C*, 2019, **7**, 2283.
43 X. Yang, Q. Wang, P. Hu, C. Xu, W. Guo, Z. Wang, Z. Mao, Z. Yang, C. Liu, G. Shi, L. Chen, B. Xu, Z. Chi. *Mater. Chem. Front.,* 2020, **4**, 941.
44 X. Feng, J. Zhang, Z. Hu, Q. Wang, M.M. Islam, J. S. Ni, M. R. J. Elsegood, J. W. Y. Lam, E. Zhou, B. Z. Tang. *J. Mater. Chem. C,* 2019, **7,** 6932.
45 X. Y. Shen, Y. J. Wang, E. Zhao, W. Z. Yuan, Y. Liu, P. Lu, A. Qin, Y. Ma, J. Z. Sun, B. Z. Tang. *J. Phys. Chem*. C, 2013, **117**, 7334.
46 Q. Yan, S. Wang. *Mater. Chem. Front.*, 2020, **4**, 3153.
47 J. Zhao, Z. Chi, Y. Zhang, Z. Mao, Z. Yang, E. Ubbaa, Z. Chi. *J. Mater. Chem. C*, 2018, **6**, 6327.
48 J. C. Ruiz-Morales, A. Tarancón, J. Canales-Vázquez, J. Méndez-Ramos, L. Hernández-Afonso, P. Acosta-Mora, J. R. Marín Rueda and R. Fernández-González, *Energy Environ. Sci.*, 2017, **10**, 846.
49 S. Xie, G. Gong, Y. Song, H. Tan, C. Zhang, N. Li, Y. Zhang, L. Xu, J. Xu and J. Zheng, *Dalton Trans.*, 2019, **48**, 6971.
50 T. Lyu and P. Dorenbos, *Chem. Mater.*, 2020, **32**, 1192.
51 46. A. Abdollahi, H. Roghani-Mamaqani, B. Razavi and M. Salami-Kalajahi, *ACS Nano*, 2020, **14**, 14417.
52 S. Yang, B. Zhou, Q. Huang, S. Wang, H. Zhen, D. Yan, Z. Lin and Q. Ling, *ACS Appl. Mater. Interfaces*, 2020, **12**, 1419.
Graphic comm. 1997, **5**, 44.
54 J. Qian. Handbook of Ink formulations and Printing. Edition (ed). China Light Industry Press, 2004, P548.
55 A. G. Crawford, A. D. Dwyer, Z. Liu, A. Steffen, A. Beeby, L. O. Palsson, D. J. Tozer and T. B. Marder, *J. Am. Chem. Soc.*, 2011, **133**, 13349.
56 M. Feckova, I. K. Kalis, T. Roisnel, P. le Poul, O. Pytela, M. Klikar, F. Robin le Guen, F. Bures, M. Fakis and S. Achelle, *Chem. Eur. J.,* 2021, **27,** *1145*.
57 E. Wang, J. W. Y. Lam, R. Hu, C. Zhang, Y. S. Zhao and B. Z. Tang, *J. Mater.Chem. C*, 2014, **2**, 1801.
58 R. R. Hu, E. Lager, A. Aguilar-Aguilar, J. Z. Liu, J. W. Y. Lam, H. H. Y. Sung, I. D. Williams, Y. C. Zhong, K. S. Wong, E. Pena-Cabrera and B. Z. Tang, *J. Phys. Chem. C*, 2009, **113**, 15845.
59 D. N. Coventry, A. S. Batsanov, A. E. Goeta, J. A. K. Howard, T. B. Marder, R. N. Perutz. *Chem. Commun*., 2005, 2172.
60 Tu Y, Liu J, Zhang H, Peng Q, Lam JWY. Tang BZ. Angew. Chem. Int. Ed. 2019; 58(42): 14911.
61 S. W. Yang, A. Elangovan, K. C. Hwang, T. I. Ho, *J Phys Chem B*, 2005, **109**: 16628.
62 J. Zhao, Z. Chi, Y. Zhang, Z. Mao, Z. Yang, E. Ubba and Z. Chi, *J. Mater.Chem. C*, 2018, **6**, 6327.
63 G. Lu, Y. Chen, Y. Zhang, M. Bao, Y. Bian, X. Li and J. Jiang, *J. Am. Chem. Soc.*, 2008, **130**, 11623.
64 Yan Yibo, Zhang J, Yi S, Liu L, Huang C. Anal. Chim. Acta. 2021; 1155: 238119
65 Saint and Sadabs; Bruker Axs Inc.: Madison, Wisconsin, USA, 2005.
66 Shelxtl Program Package, Version 5.1; Bruker Axs, Inc: Madison, WI, 1997.
67 k M. Sheldric SHELX-97 - Programs for crystal structure determination (SHELXS) and refinement (SHELXL), Acta Cryst. 2008, **A64**, 112.
68 S. P. Westrip, J. Appl. Cryst., 2010, *43,* 920.
69 Z. Hu, Y. Li, M. Kang, M. M.Islam, M. Chen, J. Zhang, Y. Xiao, X. Feng, C. Redshaw, M. Zhang, Q. Chen, S. Xie J. W. Y. , Lam, B. Z. Tang, *EcoMat*., 2020, 1.
70 A. Kathiravan, V. Srinivasan, T. Khamrang, M. Velusamy, M. Jaccob, N. Pavithra, S. Anandan, K. Velappan. *Phys. Chem. Chem. Phys.*, 2017, 19, 3125.